A&A 675, L9 (2023)
https://doi.org/10.1051/0004-6361/202245721

Astronomy & Astrophysics

LETTER TO THE EDITOR

Carbynes connected to polycyclic aromatic hydrocarbons as potential carriers of diffuse interstellar bands

Zeila Zanolli[1], Osman Barış Malcıoğlu[2], and Jean-Christophe Charlier[3]

[1] Chemistry Department, Debye Institute for Nanomaterials Science, Condensed Matter and Interfaces, Utrecht University, European Theoretical Spectroscopy Facility (ETSF), PO Box 80.000, 3508 TA Utrecht, The Netherlands
e-mail: z.zanolli@uu.nl
[2] Physics Department, Middle East Technical University, 06800 Çankaya Ankara, Turkey
[3] Université catholique de Louvain (UCLouvain), Institute of Condensed Matter and Nanosciences, Chemin des étoiles 8, 1348 Louvain-la-Neuve, Belgium
e-mail: jean-christophe.charlier@uclouvain.be

Received 19 December 2022 / Accepted 21 June 2023

ABSTRACT

Diffuse insterstellar bands (DIBs) are absorption features in the spectra of reddened stars, caused by the absorption of light by the interstellar medium. Organic molecules based on polycyclic aromatic hydrocarbons (PAHs), revealed by infrared emission bands, are present in the interstellar medium and are considered to be possibly responsible for DIBs. However, the specific carbon-based nanostructures are still unidentified, with the notable exception of C_{60}^{+} (Campbell et al. 2015, Nature, 523, 322). In the present work, using state-of-the-art time-dependent density functional theory (TDDFT) and many-body perturbation theory within the GW approximation, we predict that carbon chains (carbynes) connected to PAH groups exhibit absorption spectra that can be tuned in the energy window of the unexplained DIB spectrum. Our theoretical results reveal electronic transitions in both the visible and near-infrared range depending on the length of the carbyne chain and the nature of the connected PAHs, thus providing new insights into the possible carbon-based species populating interstellar space.

Key words. ISM: lines and bands – ISM: molecules – methods: numerical

1. Introduction

Diffuse interstellar bands (DIBs) are due to the absorption of light by the interstellar medium, observed against the background of a source of visible light (Fan et al. 2019). They were first reported one hundred years ago by the astronomer Mary Lea Heger (Heger 1919, 1922; Merrill 1934; Herbig 1995), and currently about 500 DIBs are catalogued (Geballe 2016), which have been observed all over the visible spectral range as well as in the near infrared, from ∼400 to ∼1800 nm (Geballe et al. 2011). However, the univocal identification of the molecular species responsible for the DIBs (namely, the carriers) constitutes one of the longest-standing mysteries of modern astronomy – with the exception of C_{60}^{+} (Campbell et al. 2015; Cordiner et al. 2019, and references therein), no carrier has firmly been identified. Identification of DIBs' carriers will provide information on the molecular species and astrochemical networks populating nebulae and protoplanetary disks enveloping stars in their early stages of life. This is crucial to understand the chemical reactions underlying the nucleation and evolution of interstellar material and, ultimately, their influences in the formation of stars and planets.

In addition to fullerenes, other organic molecules are populating interstellar clouds. Polycyclic aromatic hydrocarbons (PAHs) are a family of planar molecules based on benzene-like building blocks, and they are definitely present in the interstellar medium (Léger et al. 1989; Tielens 2008). After the existence of interstellar PAH compounds was revealed by the analysis of infrared (IR) emission bands (Leger & Puget 1984; Allamandola et al. 1985), PAH molecules were proposed as DIB carriers (Crawford et al. 1985; Léger & D'Hendecourt 1985; van der Zwet & Allamandola 1985).

Pure carbon chain molecules (formula l-C_N) have also been suggested as DIBs' carriers following the discovery of linear molecules in dense clouds (Douglas 1977; Mitchell & Huntress 1979). A recent study on the nature of interstellar matter proposes a combination of amorphous organic solids with a mixed aromatic-aliphatic structure to explain the unidentified and the aromatic infrared emission bands (Kwok & Zhang 2011; Chiar et al. 2013). However, there is presently no systematic agreement as to the comparison between the DIBs and the spectral features of all these carbon-based molecules. The unambiguous experimental identification of DIBs is an extremely challenging task, as laboratory conditions have to mimic the ultralow pressure and cryogenic temperature characteristic of the interstellar medium. Due to the complexity of laboratory measurements, theoretical modelling is needed to screen and to possibly identify other suitable candidates.

In this work, following up on a study of dinaphthylpolyynes by Cataldo et al. (2010), we propose that linear carbon chains (carbynes) stabilized by PAH groups attached at both ends are possible components of the interstellar medium. The optical absorption spectrum of specific PAH–carbyne–PAH compounds is computed within time-dependent density functional

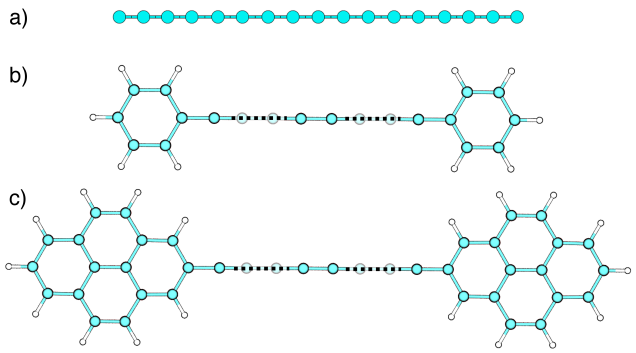

Fig. 1. Ball-and-stick models of a linear carbon chain C_{2n} (a), a doubly phenyl-capped chain (b), and a doubly pyrenyl-capped chain (c). Carbon atoms are coloured in light blue, and hydrogen atoms are in white. Bonds are represented only for visual aid as single sticks that are not indicative of bond order.

theory (TDDFT; Runge & Gross 1984; Marques et al. 2006; Casida et al. 2009) and tested against a parameter-free approach based on the GW approximation and the Bethe-Salpeter equation (BSE; Hedin 1965; Hybertsen & Louie 1986; Aryasetiawan & Gunnarsson 1998; Onida et al. 2002; Strinati 1988). This investigation reveals intense electronic transitions in the visible and near-IR which vary systematically with the length of the carbyne chain and the nature of the connected PAHs. This family of carbon-based molecules (and networks) are analysed as possible new DIB carriers.

2. Methods

The calculations of the optical absorption spectra of linear carbon chains (C_{2n}), both pure and terminated with benzene (C_6H_6–C_{2n}–C_6H_6 or C_{2n}-2B) or pyrene ($C_{16}H_{10}$–C_{2n}–$C_{16}H_{10}$ or C_{2n}-2P) with $2n$ ranging from four to 30, have been performed using the time-dependent DFT formalism within Casida's formulation. The systems under investigation are illustrated in Fig. 1. Ground-state DFT and TDDFT calculations have been performed with the NWChem package (Valiev et al. 2010). For the sake of comparison, neutral excitation energies have also been calculated within a combined many-body perturbation theory GW/BSE formalism using the Fiesta package (Blase et al. 2011; Faber et al. 2011, 2012). All the calculations have been performed without resorting to the Tamm–Dancoff approximation (TDA), since this approximation breaks down in π-conjugated molecules (Grüning et al. 2009). Theoretical and computational details are reported in Appendices B and C.

3. Results and discussion

3.1. Ground state and stability

Carbynes are linear carbon chains with sp orbital hybridization (Fig. 1a), which can present an alternation of single and triple bonds (polyyne) or consecutive double bonds (cumulene). Energetic stability of carbynes can be achieved by bonding their extremities to sp^2 or sp^3 carbon atoms from various carbon-based nanostructures such as graphene-like fragments or fullerene-like structures, respectively (see Appendix A). When this occurs, the ideal single-triple or double-double bond sequence is altered. The bonding of a carbon chain with two PAH groups occurs via a single σ bond. Hence the PAH–carbyne–PAH systems tend to develop single-triple bond alternation in the chain. This can easily be achieved when the chain consists of an even number of C atoms C_{2n}-2PAH leaving no unpaired electrons and resulting in a spin singlet ground state (closed shell configuration). Alternatively, C_{2n+1}-2PAH structures, which contain an odd number of carbon atoms in the chain, cannot consist of an integer number of single-triple bonds and present double bonds in the middle of the chain. In C_{2n+1}-2PAH structures, two electrons with the same spin orientation are delocalized over the entire chain (Zanolli et al. 2010) giving a total magnetic moment of $2\mu_B$ and resulting in an open shell configuration with a spin triplet ground state (spin magnetic moment $S = 1$), as also found in the present DFT calculations. Since open shell systems are not easily described in TDDFT or in GW/BSE, this work focusses on closed shell systems such as C_{2n}-2PAH.

Possible DIB's carriers are molecules characterized by electronic transitions in the 400−1800 nm range involving π–$\pi^\star$ excitations with a large oscillator strength (e.g., $f \geq 1$) and a long lifetime in the excited state (≥70 fs) (Maier 1998; Rice & Maier 2013). Since it is well known[1] (Salem 1966) that the wavelength and oscillator strength of these π–$\pi^\star$ transitions increase quasi-linearly with the number of carbon atoms in linear C_{2n}–based molecules, the first two conditions can be met by increasing n.

In addition, it has been shown experimentally (Maier 1998) that neutral carbon chains consisting of an even number of carbon atoms C_{2n} exist in the linear geometry only up to $n = 5$, which is not enough to reach the DIBs' region. Longer C_{2n} chains are monocyclic and have been excluded as DIBs' carriers (Yang et al. 1988; Handschuh et al. 1995; Wakabayashi et al. 1997). Odd-numbered chains C_{2n+1} with $n \geq 8$ have been suggested as possible candidates. However, no emission was observed, possibly due to a lifetime of the excited state that was too short (Rice & Maier 2013). For this reason, in order to narrow the number of possible DIBs' carriers, other candidates need to be investigated, such as the series of C_{2n}-2PAH molecules.

3.2. Optical spectra of C_8-2B

The first absorption peak of the C_8-2B molecule (Fig. 1b) is near the onset of the DIBs' region (~400 nm), as predicted by our GW/BSE and TDDFT optical spectra (Fig. 2). One can expect that, analogously to the trend observed in simpler C_{2n}-based molecules, the energy of the first relevant transition of this and other C_{2n}-2PAH molecules will move deeper in the DIBs' range by increasing n. Indeed, this trend has been observed and predicted via empirical models in the 1970s (Nakasuji et al. 1972; Akiyama et al. 1973). Within both theories, only the second and seventh excitations have a non-zero oscillator strength. The former is mostly contributed to by the HOMO → LUMO transition, and the latter by the HOMO−1 → LUMO+1. Hence, in the optical spectrum of C_8-2B (reported in Fig. 2), the two lowest energy peaks at 3.2 eV and 4.8 eV can be ascribed to the HOMO → LUMO and HOMO−1 → LUMO+1 transition, respectively. These peaks are specific features of this complex molecule and are not observed in isolated chains or benzene: the computed TDDFT excitation spectra of C_6H_6 and a

[1] The observed quasi-linear dependence between the wavelength of the HOMO–LUMO transition and the number N of carbon atoms in most of the C_N–based molecules can be understood with a one-dimensional particle in a box model for π electrons in which the size of the box is proportional to the chain length (Salem 1966). However, further experiments (Pino et al. 2001) show that this dependence is exponential for neutral polyynes chains, such as $HC_{2n}H$.

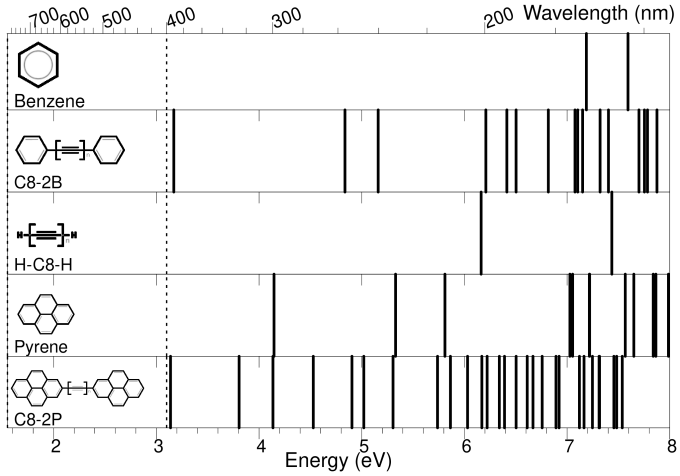

Fig. 2. Singlet root energies from TDDFT for the individual components of two C_8-2PAH systems (C_8-2B and C_8-2P), pyrene ($C_{16}H_{10}$), benzene (C_6H_6), and the doubly H-terminated C_8 chain. Dipole oscillator strengths less than 0.01 are omitted in the graph. The vertical dashed line indicates the onset of the DIBs' region that extends from ∼400 to ∼1800 nm.

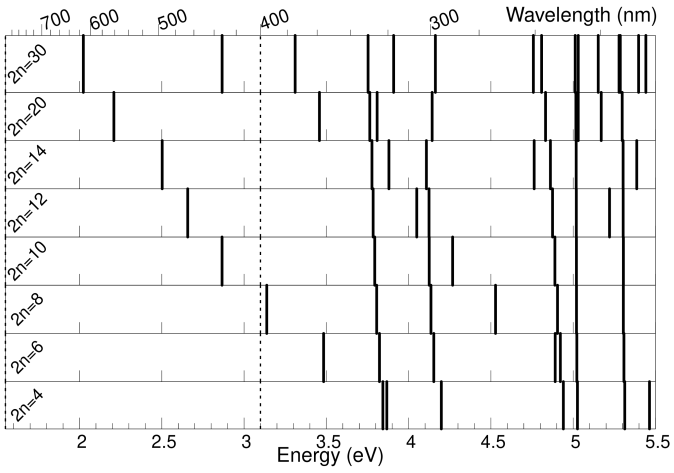

Fig. 3. Singlet root energies of the C_{2n}-2P molecules, with $2n$ = 4–30. The onset of the DIBs' region (∼400 nm) is indicated by the dashed line. Transitions with dipole oscillator strengths less than 0.01 are omitted.

H-terminated C_8 molecule fall in the UV region (Fig. 2). The HOMO → LUMO transition of the HC_8H molecule ($X^1\Sigma_g^+ \rightarrow {}^1\Sigma_u^+$, as follows from spin and dipole selection rules) is responsible for a strong absorption peak in the UV at 6.16 eV, which compares well with the experimental result at 5.98 eV (Kloster-Jensen et al. 1974). The first relevant transition for benzene (7.19 eV) also compares well with absorption experiments (Pantos et al. 1978), which reveal a very intense peak at ∼6.96 eV due to the $\pi \rightarrow \pi^\star$ ($^1A_{1g} \rightarrow {}^1E_{1u}$) transition. In addition, inspection of the Kohn-Sham DFT wave functions of the molecular levels (Fig. B.1) shows that HOMO, LUMO, and, to a lesser extent, HOMO−1 and LUMO+1 states are delocalized over the whole system, that is on both the chain and benzene terminations.

Overall, the optical absorption spectra of C_8-2B computed with TDDFT and GW/BSE approaches are in excellent agreement for both ordering and the character of the optical excitation energies (Appendix D). We find that TDDFT tends to locate the excitation energies slightly higher than GW/BSE with a difference ranging from ∼0.06 eV to ∼0.16 eV for the three lowest excited states. The discrepancies increase to about 0.3–0.4 eV from the fourth to the seventh excited state. The difference in the computed transition energies can be due to the CAM-PBE0 functional parameters, which have not been optimized for the present family of systems. The original default values of Rohrdanz & Herbert (2008) were used instead. Indeed, a study of cyanine chains (Boulanger et al. 2014) shows that TDDFT calculations with local, global, or range-separated hybrid functionals similarly overestimate the transition energies as compared to GW/BSE calculations and *exCC*3 high-level quantum chemistry calculations, showing evidence of the importance of explicitly including non-local correlation contributions in addition to non-local exchange.

3.3. Optical spectra of C_{2n}-2P

The correct ordering of the excitations and the excellent agreement between TDDFT and GW/BSE for the lowest energy excitations is a strong confirmation that TDDFT calculations with range-separated hybrid functionals provide a reliable description of the excitation spectrum of these systems. Hence the TDDFT approach was used to model more complex C_n–PAH systems, such as the series of C_{2n}-2P molecules (Fig. 1c). Figure 2 shows that the PAHs linked with carbon chains have a low-energy spectral footprint, distinct from both the hydrogen-terminated chain and the PAHs. The spectral fingerprint of the PAHs remains the same when linked to the chain. Analogously to the C_8-2B case, the TDDFT spectrum of C_8-2P (Fig. 2) also presents two peaks at low energy (at 3.14 eV – at the edge of the DIB zone – and at 4.53 eV) characteristic of the C_8-2P molecule. This is revealed by direct comparison with the TDDFT spectra of isolated pyrene and the H–C_8–H molecule, which absorb in the UV (Fig. 2). Indeed, the three lowest energy peaks of pyrene were computed at 4.15 eV, 5.33 eV, and 5.81 eV, and they are in a reasonable agreement with the experimental values (3.71 eV, 4.56 eV, and 5.19 eV) (Johnson & Asher 1984; Salama & Allamandola 1993; Halasinski et al. 2005) and can be clearly distinguished from the C_8-2P peaks in Fig. 2.

Figure 3 shows that the low-energy fingerprint of PAHs that is interlinked with carbon chains have a strong dependence on the length of the chain, going to lower energies as the chain size increases, which is in agreement with experimental measurements of Nakasuji et al. (1972) and Akiyama et al. (1973). The spectral footprint of the terminating PAHs remains almost unchanged. The peaks that can be ascribed to the pyrene terminations are present in the whole C_{2n}-2P ($2n$ = 4−30) series at roughly the same energy (Fig. 3). By contrast, the two peaks characteristic of the C_8-2P molecule are found to shift towards longer wavelengths with increasing n (Fig. 3). In particular, the low-energy peak moves further into the DIBs' region with a quasi-linear trend for small n, before tending to a possible asymptotic behaviour (Fig. 4). This behaviour is similar to what has been observed in H–C_{2n}–H (Pino et al. 2001). However, while the H–C_{2n}–H series does not reach the DIB zone, the current C_{2n}-2P series falls between 400 nm ($2n$ = 8) and 600 nm ($2n$ = 30), which is well within the region of interest.

According to the trend observed in experiments for the C_N-based molecules (Maier 1998; Pino et al. 2001; Rice & Maier 2013), one would also expect the oscillator strength of the low-energy excitations to increase with N. However, this is

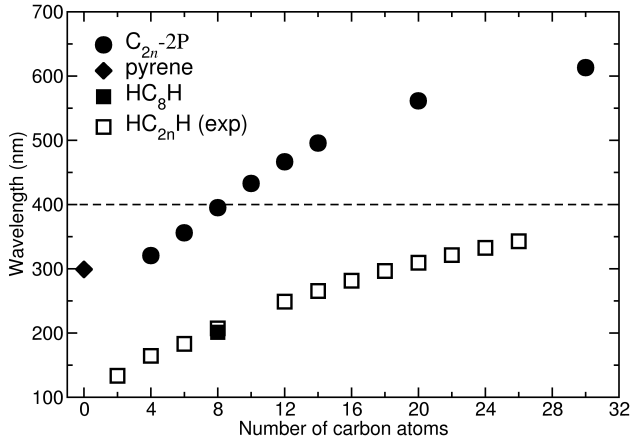

Fig. 4. Evolution of the first absorption peak of the C_{2n}-2P series computed within TDDFT (circles) with the number of carbon atoms. For comparison, computed values for pyrene (diamond), HC_8H (filled square), and experimental data from Pino et al. (2001) for $HC_{2n}H$ (open squares) are reported. DIBs are observed at wavelengths longer than 400 nm, that is to say above the dashed line.

not the case for the C_{2n}-2P series. A detailed analysis of the excitations with non-zero oscillator strength (Appendix E) show that the main contribution to the two low-energy peaks changes with n. For $2n = 4$ and 6, the first and second relevant (i.e., characteristic of the C_{2n}-2P molecule) peaks are mostly due to a single transition from occupied to empty states. By increasing n, each of these excitations is mostly contributed to by two transitions (see Table E.1). Hence, the oscillator strength includes an interference term given by the product of the amplitudes and of the dipole moments of each contributing transition. By increasing n, all the transitions contribute comparably, leading to destructive interference for the first excitation and a constructive one for the second.

4. Conclusion

In conclusion, combined GW/BSE and TDDFT calculations on a series of C_{2n}-2PAH molecules have been used to interpret their complex absorption spectra. Similar systems have been investigated experimentally and using empirical models (Nakasuji et al. 1972; Akiyama et al. 1973) or ground-state DFT simulations (Cataldo et al. 2010). The trend we predict is in agreement with these experiments. The new information brought by this study is a consequence of the higher accuracy of the theoretical and computational techniques (GW/BSE and TDDFT). These techniques fully include, for the first time, the direct effect of the PAH on the chains' optical properties (rather than a shift of the frontier electronic levels of the chain).

Among the many absorption features, two low-energy excitations that are characteristic of the C_{2n}-2PAH molecules have been identified. The absorption energy of both excitations decrease with n, bringing the first peak into the DIB region. However, the oscillator strength of this excitation decreases with n, making the possibility of achieving an experimental observation of this excitation unlikely. The oscillator strength of the second peak, instead, increases with n, but the position of the peak does not reach the DIB zone, except for the long C_{30}-2P molecule.

This investigation shows that the combination of a sp system (the linear carbon chain) with sp^2 ones (the PAH groups) can push the absorption spectra towards the DIB zone, which cannot be achieved by the individual molecules. This information, combined with the recent assignment (Campbell et al. 2015) of two DIBs at ~9578 Å and ~9633 Å to C_{60}^+, indicates that possible DIBs' carriers could be found in the series of linear C_{2n} chains connecting two fullerene-like molecules. Another possible future direction could be the study of C_{2n}-2PAH$^+$ ions, considering that DIB carriers could be ionized by the interstellar radiation field, in analogy to C_{60}^+. It should be noted that the presence of C_{2n}-2PAH molecules in the interstellar medium could be explained by complex chemical reactions and an interaction with the interstellar radiation field, which is beyond the scope of this work.

Lastly, these theoretical predictions provide new insights into the specific carbon-based species populating interstellar space. They hence open the way to the identification of chemical networks in protoplanetary disks surrounding stars in their early stages of life, and they drive the understanding of the nucleation and growth of interstellar dust and, possibly, its specific role in star and planet formation.

Acknowledgements. The authors acknowledge support from the NanoSpace COST action (CA21126 – European Cooperation in Science and Technology) and scientific discussions with Carina Faber, Paul Boulanger, Xavier Blase, Nicolas Dardenne, Gian-Marco Rignanese, and Chris Ewels at the early stages of the present research. ZZ acknowledges financial support by the Netherlands Sector Plan program 2019–2023 and from the research program "Materials for the Quantum Age" (QuMAT, registration number 024.005.006), part of the Gravitation program of the Dutch Ministry of Education, Culture and Science (OCW). JCC acknowledges financial support from the European Union's Horizon 2020 Research Project and Innovation Program – Graphene Flagship Core3 (N° 881603), from the Fédération Wallonie-Bruxelles through the ARC Grant (N° 21/26-116), from the EOS project "CONNECT"? (N° 40007563), and from the Belgium F.R.S.-FNRS. Computational resources have been provided by the CISM supercomputing facilities of UCLouvain, the CÉCI consortium funded by F.R.S.-FNRS of Belgium (N° 2.5020.11), and also subsidized by NWO-Domain Science.

References

Akiyama, S., Takeuchi, Y., Yasuhara, A., Nakagawa, M., & Nishimoto, K. 1973, Bull. Chem. Soc. Jpn., 46, 2830
Allamandola, L. J., Tielens, A. G. G. M., & Barker, J. R. 1985, ApJ, 290, L25
Aryasetiawan, F., & Gunnarsson, O. 1998, Rep. Prog. Phys., 61, 237
Baumeier, B., Andrienko, D., Ma, Y., & Rohlfing, M. 2012, J. Chem. Theory Comput., 8, 997
Becke, A. D. 1993, J. Chem. Phys., 98, 1372
Benedict, L. X., Shirley, E. L., & Bohn, R. B. 1998, Phys. Rev. Lett., 80, 4514
Blase, X., Attaccalite, C., & Olevano, V. 2011, Phys. Rev. B: Condens. Matter Mater. Phys., 83, 115103
Boulanger, P., Jacquemin, D., Duchemin, I., & Blase, X. 2014, J. Chem. Theory Comput., 10, 1212
Campbell, E. K., Holz, M., Gerlich, D., & Maier, J. P. 2015, Nature, 523, 322
Cardona, M., Lastras-Martínez, L. F., & Aspnes, D. E. 1999, Phys. Rev. Lett., 83, 3970
Casida, M. E., Chermette, H., & Jacquemin, D. 2009, J. Mol. Struct., 914, 1
Cataldo, F., Ravagnan, L., Cinquanta, E., et al. 2010, J. Phys. Chem. B., 114, 14834
Chalifoux, W. A., & Tykwinski, R. R. 2010, Nat. Chem., 2, 967
Chiar, J. E., Tielens, A. G., Adamson, A. J., & Ricca, A. 2013, Astrophys. J., 770, 78
Cordiner, M. A., Linnartz, H., Cox, N. L. J., et al. 2019, ApJ, 875, L28
Crawford, M. K., Tielens, A. G. G. M., & Allamandola, L. J. 1985, ApJ, 293, L45
Douglas, A. E. 1977, Nature, 269, 130
Ernzerhof, M., & Scuseria, G. E. 1999, J. Chem. Phys., 110, 5029
Faber, C., Attaccalite, C., Olevano, V., Runge, E., & Blase, X. 2011, Phys. Rev. B: Condens. Matter Mater. Phys., 83, 115123
Faber, C., Duchemin, I., Deutsch, T., & Blase, X. 2012, Phys. Rev. B: Condens. Matter Mater. Phys., 86, 155315
Faber, C., Boulanger, P., Duchemin, I., Attaccalite, C., & Blase, X. 2013, J. Chem. Phys., 139, 194308
Fan, H., Hobbs, L. M., Dahlstrom, J. A., et al. 2019, ApJ, 878, 151

Farid, B., Daling, R., Lenstra, D., & Van Haeringen, W. 1988, Phys. Rev. B, 38, 7530
Geballe, T. R. 2016, J. Phys: Conf. Ser., 728, 062005P
Geballe, T. R., Najarro, F., Figer, D. F., Schlegelmilch, B. W., & de la Fuente, D. 2011, Nature, 479, 200
Gibtner, T., Hampel, F., Gisselbrecht, J. P., & Hirsch, A. 2002, Chem. Eur. J., 8, 408
Godby, R. W., Schlüter, M., & Sham, L. J. 1988, Phys. Rev. B, 37, 10159
Grüning, M., Marini, A., & Gonze, X. 2009, Nano Lett., 9, 2820
Halasinski, T. M., Salama, F., & Allamandola, L. J. 2005, ApJ, 628, 555
Handschuh, H., Ganteför, G., Kessler, B., Bechthold, P. S., & Eberhardt, W. 1995, Phys. Rev. Lett., 74, 1095
Hanke, W., & Sham, L. J. 1979, Phys. Rev. Lett., 43, 387
Hedin, L. 1965, Phys. Rev., 139, A796
Heger, M. L. 1919, Lick Obs. Bull., 10, 59
Heger, M. L. 1922, Lick Obs. Bull., 10, 141
Herbig, G. H. 1995, ARA&A, 33, 19
Hybertsen, M. S., & Louie, S. G. 1986, Phys. Rev. B, 34, 5390
Johnson, C. R., & Asher, S. A. 1984, Anal. Chem., 56, 2258
Kloster-Jensen, E., Haink, H., & Christen, H. 1974, Helv. Chim. Acta, 57, 1731
Kowalski, K., Krishnamoorthy, S., Villa, O., Hammond, J. R., & Govind, N. 2010, J. Chem. Phys., 132, 154103
Kwok, S., & Zhang, Y. 2011, Nature, 479, 80
Lange, A. W., Rohrdanz, M. A., & Herbert, J. M. 2008, J. Phys. Chem. B, 112, 7345
Leger, A., & Puget, J. L. 1984, A&A, 137, L5
Léger, A., & D'Hendecourt, L. 1985, A&A, 146, 81
Léger, A., d'Hendecourt, L., & Défourneau, D. 1989, A&A, 216, 148
Maier, J. P. 1998, J. Phys. Chem. A, 102, 3462
Marques, M. A., Ullrich, C. A., Nogueira, F., et al. 2006, in Time-Dependent Density Functional Theory (Berlin: Springer), Lecture Notes in Physics, 706
Merrill, P. W. 1934, PASP, 46, 206
Mitchell, G. F., & Huntress, W. T. 1979, Nature, 278, 722
Nakasuji, K., Akiyama, S., & Nakagawa, M. 1972, Bull. Chem. Soc. Jpn., 45, 875
Onida, G., Reining, L., & Rubio, A. 2002, Rev. Mod. Phys., 74, 601
Pantos, E., Philis, J., & Bolovinos, A. 1978, J. Mol. Spectrosc., 72, 36
Pino, T., Ding, H., Güthe, F., & Maier, J. P. 2001, J. Chem. Phys., 114, 2208
Ravagnan, L., Manini, N., Cinquanta, E., et al. 2009, Phys. Rev. Lett., 102, 245502P
Rice, C. A., & Maier, J. P. 2013, J. Phys. Chem. A, 117, 5559
Rohlfing, M., & Louie, S. G. 1998, Phys. Rev. Lett., 80, 3320
Rohrdanz, M. A., & Herbert, J. M. 2008, J. Chem. Phys., 129, 034107P
Runge, E., & Gross, E. K. 1984, Phys. Rev. Lett., 52, 997
Sadlej, A. J. 1988, Collect. Czech. Chem. Commun., 53, 1995
Salama, F., & Allamandola, L. J. 1993, J. Chem. Soc., Faraday Trans., 89, 2277
Salem, L. 1966, Molecular Orbital Theory of Conjugated Systems No. 6 (Reading, Massachusetts: W. A. Benjamin)
Schuchardt, K. L., Didier, B. T., Elsethagen, T., et al. 2007, J. Chem. Inf. Model., 47, 1045
Sham, L. J., & Rice, T. M. 1966, Phys. Rev., 144, 708
Sharifzadeh, S., Tamblyn, I., Doak, P., Darancet, P. T., & Neaton, J. B. 2012, Eur. Phys. J. B, 85, 323
Strinati, G. 1982, Phys. Rev. Lett., 49, 1519
Strinati, G. 1988, La Rivista Del Nuovo Cimento Series, 3(11), 1
Tiago, M. L., Idrobo, J. C., Öğüt, S., Jellinek, J., & Chelikowsky, J. R. 2009, Phys. Rev. B: Condens. Matter Mater. Phys., 79, 155419
Tielens, A. G. G. M. 2008, ARA&A, 46, 289
Valiev, M., Bylaska, E. J., Govind, N., et al. 2010, Comput. Phys. Commun., 181, 1477
van der Zwet, G. P., & Allamandola, L. J. 1985, A&A, 146, 76
Wakabayashi, T., Kohno, M., Achiba, Y., et al. 1997, J. Chem. Phys., 107, 4783
Yang, S., Taylor, K. J., Craycraft, M. J., et al. 1988, Chem. Phys. Lett., 144, 431
Zanolli, Z., Onida, G., & Charlier, J. C. 2010, ACS Nano, 4, 5174

Appendix A: Stability

Uncapped monoatomic carbon chains (C_{2n} and C_{2n+1}) are known to be highly reactive. However, energetic stability of carbon chains can be achieved by bonding their extremities to sp^2 or sp^3 C-based fragments, as predicted by DFT simulations (Ravagnan et al. 2009) and experiments (Chalifoux & Tykwinski 2010; Gibtner et al. 2002). In order to assess the stability of the mixed aromatic-aliphatic organic molecules presented in this work, with DFT, we computed the binding energy of the C_8 chain doubly terminated with H, benzene, and pyrene with respect to the bare C_8 chain as follows:

$$E_b(HC_8H) = E(HC_8H) - E(H_2) - E(C_8),$$
$$E_b(C_8\text{-}2B) = E(C_6H_5C_8C_6H_5) - 2E(C_6H_6) - E(C_8) + E(H_2),$$
$$E_b(C_8\text{-}2P) = E(C_{16}H_9C_8C_{16}H_9) - 2E(C_{16}H_{10}) - E(C_8) + E(H_2).$$

The obtained binding energies (Table A.1) are negative and, hence, consistent with this picture: an uncapped carbon chain is energetically stable when adding hydrogen atoms or PAH groups to its extremities. We find that the stabilization decreases with increasing size of the PAH fragment, which is consistent with the experimental findings of Gibtner et al. (2002).

Table A.1. Computed binding energy of the C_8 chain doubly terminated with H, benzene, and pyrene with respect to the bare C_8 chain.

system	$E_{binding}$ (eV)
$H - C_8 - H$	-8.235
$C_6H_5 - C_8 - C_6H_5$	-7.838
$C_{16}H_9 - C_8 - C_{16}H_9$	-7.808

Appendix B: Time-dependent DFT

Ground-state DFT and excited-state TDDFT calculations have been performed using the NWChem code (Valiev et al. 2010). Once the DFT Kohn-Sham ground-state single-particle wavefunctions and eigenvalues are calculated, this effective two-particle representation allows one to directly access electron-hole excitation energies, the corresponding oscillator strengths, and the character of the transitions. The nature of the electron-hole interactions is controlled by the choice of the exchange-correlation kernel. A visual representation of Kohn-Sham DFT wave functions for a C_8-2B molecule is given in Fig. B.1.

All the investigated structures have been relaxed using the B3LYP functional (Becke 1993), an aug-cc-pvdz basis set (Schuchardt et al. 2007, and references therein) and default NWChem convergence criteria. The ground-state geometry exhibits a D_{2H} point group symmetry. Ground-state DFT Kohn-Sham wave functions and eigenvalues were then computed. The latter values are used as a starting point for the calculation of TDDFT optical excitation spectra, which is performed using a Coulomb attenuated long range corrected functional CAM-PBE0 (Lange et al. 2008; Kowalski et al. 2010), still using an aug-cc-pvdz basis as the vertical excitation spectra are more stable than other spectroscopical observables with respect to the basis size because of error cancellation between the electron and hole contributions. The excitation energies of the spectral features computed with a triple zeta basis set (Sadlej 1988) differ by only ~0.01 eV from those obtained with the aug-cc-pvdz basis. A Gaussian broadening of 0.01 eV is applied to the spectral peaks.

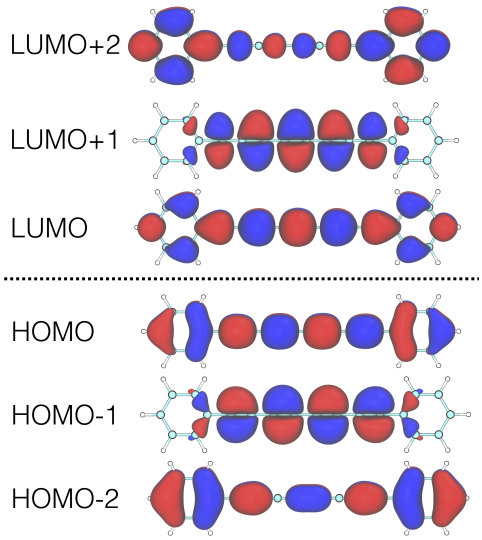

Fig. B.1. Isodensity contours' representation of the Kohn-Sham DFT wave functions of the three highest occupied and the three lowest unoccupied molecular levels, which mostly contribute to the lowest lying optical excitations of a C_8-2B molecule. These Kohn-Sham wave functions have been used as starting point for TDDFT and *GW*/BSE calculations.

Appendix C: Many-body perturbation theory *GW*/BSE

For the sake of comparison, neutral excitation energies are also calculated within a combined many-body perturbation theory *GW*/BSE formalism. As a first step, the electronic structure is obtained by solving the quasi-particle equation, an effective non-linear one-particle eigenvalue equation accounting for many-body exchange and correlation effects. Starting from DFT Kohn-Sham eigenstates ψ^{KS} and eigenvalues ε^{KS}, quasi-particle energies ε^{qp} are calculated to first order in the following perturbation:

$$\varepsilon_i^{qp} \approx \varepsilon_i^{KS} + Z_i \left\langle \psi_i^{KS} \middle| \Sigma\left(\varepsilon_i^{KS}\right) - V_{xc} \middle| \psi_i^{KS} \right\rangle . \tag{C.1}$$

We note that V_{xc} represents the (semi-)local Kohn-Sham exchange-correlation functional, and Z_i denotes a renormalization factor. The self-energy Σ accounts for all exchange and correlation effects beyond Hartree. It is a non-local and energy-dependent operator and usually computed in the GW approximation (Hedin 1965; Hybertsen & Louie 1986; Godby et al. 1988; Onida et al. 2002; Aryasetiawan & Gunnarsson 1998):

$$\Sigma^{GW}(\mathbf{r}, \mathbf{r}', \omega) = \int d\omega' \, e^{i\omega' 0^+} G(\mathbf{r}, \mathbf{r}', \omega + \omega') \, W(\mathbf{r}, \mathbf{r}', \omega') , \tag{C.2}$$

where G is the time-ordered single-particle Green's function, and W is the screened Coulomb potential. In a second step, electron-hole interactions are included via the Bethe-Salpeter formalism (Sham & Rice 1966; Hanke & Sham 1979; Strinati 1982; Rohlfing & Louie 1998; Benedict et al. 1998; Cardona et al. 1999) in order to access optical excitation energies. The latter energies are obtained by solving an eigenvalue equation for the

electron-hole BSE Hamiltonian H^{e-h} expressed in a two-body Kohn-Sham product basis $\psi_e^{KS}(\mathbf{r})\psi_h^{KS}(\mathbf{r}')$:

$$\begin{pmatrix} R_{vc,v'c'} & C_{vc,c'v'} \\ -C^*_{cv,v'c'} & -R^*_{cv,c'v'} \end{pmatrix} \begin{bmatrix} X_{v'c'} \\ Y_{c'v'} \end{bmatrix} = \Omega \begin{bmatrix} X_{vc} \\ Y_{cv} \end{bmatrix}. \tag{C.3}$$

The first diagonal block, R, accounts for resonant transitions from occupied (indexed v, v') to unoccupied (indexed c, c') eigenstates and is composed of a diagonal, a direct, and an exchange part with the following contributions:

$$\begin{aligned} R &= R^{diag}_{vc,vc} + R^{direct}_{vc,v'c'} + R^{exch}_{vc,v'c'} \\ &= \left(\varepsilon_c^{GW} - \varepsilon_v^{GW}\right)\delta_{vv'}\delta_{cc'} \\ &\quad - \iint d^3\mathbf{r}d^3\mathbf{r}'\phi_v(\mathbf{r})\phi_c^*(\mathbf{r}')\, W_{st}(\mathbf{r}',\mathbf{r})\, \phi_{v'}^*(\mathbf{r}')\phi_{c'}(\mathbf{r}) \\ &\quad + 2\iint d^3\mathbf{r}d^3\mathbf{r}'\phi_v(\mathbf{r})\phi_c^*(\mathbf{r})\, v(\mathbf{r},\mathbf{r}')\, \phi_{v'}^*(\mathbf{r}')\phi_{c'}(\mathbf{r}'). \end{aligned}$$

We note that W_{st} represents the static limit of the screened Coulomb potential $W(\mathbf{r}t,\mathbf{r}'t') \rightarrow W_{st}(\mathbf{r},\mathbf{r}')\delta(t-t')$, a common approximation to make the BSE formalism computationally feasible. The remaining block elements of the BSE Hamiltonian are the non-resonant R^* part representing transitions from unoccupied to occupied states and the off-diagonal $C^{(*)}$ blocks, which couple resonant to non-resonant transitions. The TDA consists in neglecting the off-diagonal coupling blocks of the BSE Hamiltonian (Eq. C.3). Since the latter approximation breaks down in nano-scaled materials and, in particular, in π conjugated molecules (Grüning et al. 2009), all the TDDFT and BSE optical calculations of this work were computed from the full Hamiltonian.

The *GW*/BSE calculations presented in this work have been performed using the Fiesta package (Blase et al. 2011; Faber et al. 2011, 2012), which is a Gaussian basis implementation of the *GW*/BSE formalisms that uses an auxiliary basis for non-local quantities such as the screened Coulomb potential. For the present calculations, the auxiliary basis consists of four $e^{-\alpha\mathbf{r}^2}$ Gaussian functions for each (s, p, d, f) channel, with an even-tempered distribution of the localization coefficients α ranging from 0.04 to 6.0 a.u. The DFT Kohn-Sham states needed to construct the starting Green's function G and the screened Coulomb potential W are calculated using the NWChem package (Valiev et al. 2010) with a PBE0 exchange-correlation functional (Ernzerhof & Scuseria 1999) and the same aug-cc-pvdz Kohn-Sham basis adopted by the TDDFT approach. Convergence tests indicate that *GW*/BSE calculations performed with an aug-cc-pvdz Kohn-Sham basis adopted by the TDDFT approach do not change the excitation energies by more than about 20 meV for the ten lowest excitation energies as compared to a much larger aug-cc-pvtz basis.

The self-energy (Eq. C.2) is explicitly evaluated by means of contour deformation techniques, that is to say beyond any plasmon pole approximation (Godby et al. 1988; Blase et al. 2011; Farid et al. 1988). A partially self-consistent scheme was applied: The obtained quasi-particle energies were reinjected in order to update the single-particle Green's function and the screened Coulomb potential, whereas the Kohn-Sham eigenstates were kept frozen. This simple self-consistent approach provides more accurate quasi-particle energies as compared to single-shot G_0W_0 calculations, and it diminishes the dependency on the chosen mean-field starting point (Blase et al. 2011; Faber et al. 2011, 2013; Tiago et al. 2009; Sharifzadeh et al. 2012; Baumeier et al. 2012). The number of conduction bands included in the BSE Hamiltonian is 160. For C_8-2B, increasing the number of virtual states from 160 to 320 to build the BSE Hamiltonian hardly changes the lowest excitation energies (tests performed with an aug-cc-pvdz Kohn-Sham basis). All the empty states, instead, enter the *GW* calculation to, for example, construct the one-particle Green's function.

Appendix D: *GW*/BSE and TDDFT comparison

In Table D.1 and Fig. D.1, a comparison between the optical excitation energies of a C_8-2B molecule computed with both TDDFT and *GW*/BSE approaches is reported. Both kinds of calculations have been performed using the same basis (aug-cc-pvdz) and without TDA. The analysis of the *GW*/BSE and TDDFT excitation spectra allowed us to identity the energy levels that mostly contribute to each transition. The agreement between the two theories is excellent for both predicted transition energies and identification of the energy levels responsible for the transitions. Only a transition with non-zero oscillator strength can actually be observed, namely transition two (HOMO → LUMO) and seven (HOMO−1 → LUMO+1).

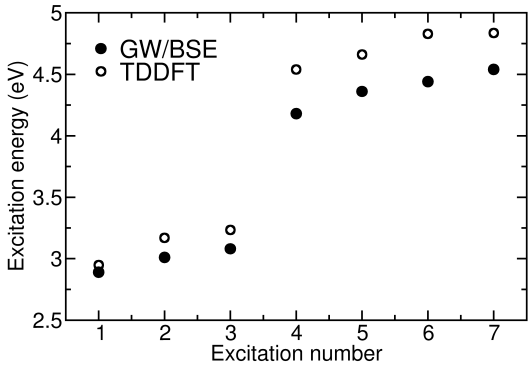

Fig. D.1. Singlet excitation energies of the C_8-2B molecule (in eV) as calculated within TDDFT and *GW*/BSE (open and filled circles, respectively). Only excitations labelled two (mostly HOMO → LUMO) and seven (mostly HOMO−1 → LUMO+1) have a non-zero oscillator strength.

Table D.1. Singlet optical excitation energies (eV) computed with *GW*/BSE and TDDFT for the C_8-2B molecule ([a]).

	Exc. Energy (eV)		Main Contribution	Oscillator Strength	
Excitation	*GW*/BSE	TDDFT	*GW*/BSE and TDDFT	*GW*/BSE	TDDFT
1	2.89	2.95	HOMO → LUMO+1	0.000	0.000
2	3.01	3.17	**HOMO → LUMO**	0.293	0.273
3	3.08	3.23	HOMO–1 → LUMO	0.000	0.000
4	4.18	4.54	HOMO–2 → LUMO+1	0.000	0.000
5	4.36	4.66	HOMO–2 → LUMO	0.000	0.000
6	4.44	4.83	HOMO–6 → LUMO	0.000	0.000
7	4.54	4.84	**HOMO–1 → LUMO+1**	3.457	4.666

Notes. Singlet optical excitation energies (eV) were computed using an aug-cc-pvdz Kohn-Sham basis set, without TDA. The fourth column indicates the principal contribution from Kohn-Sham occupied to virtual orbitals to the excitation eigenvectors. Only transitions two (HOMO → LUMO) and seven (HOMO−1 → LUMO+1) have a non-zero oscillator strength (columns 7 and 8) in both theories, reported in bold in the table. We note the excellent agreement between the TDDFT and *GW*/BSE calculations.

Appendix E: Details of the C_{2n}-2P spectra

In the TDDFT absorption spectra of the C_n-2P series, one can identify two peaks at low energy that are characteristic of the molecule and shift with n. The details (energy, oscillator strength, main contributions, etc.) of these excitations are reported in Table E.1. The other peaks, instead, can be ascribed to the pyrene terminations and, hence, do not change with n.

In the $2n = 4$ and 6 cases, the two relevant excitations at the lowest energy are mostly contributed to by a single couple of occupied and empty levels, that is the wavefunction of the excitation can be approximated by a single determinant

$$|\psi\rangle \approx A_1 \left|\psi^{(1)}\right\rangle \tag{E.1}$$

and the corresponding transition dipole moment is

$$d = \psi_{GS}\,\mathbf{r}\psi \approx A_1 \psi_{GS}\,\mathbf{r}\psi^{(1)} = d_1. \tag{E.2}$$

Hence, the oscillator strength of the excitation is

$$\begin{aligned} f &= 2(E - E_{GS})d^2 \\ &\approx 2(E - E_{GS})\,|A_1|^2 \left|\psi_{GS}\,\mathbf{r}\psi^{(1)}\right|^2, \end{aligned} \tag{E.3}$$

which increases with the length of the molecule. Indeed, the present TDDFT calculations predict that the oscillator strength of the two low-energy excitations increases from C_4-2P to C_6-2P (Table E.1). This is also in agreement with the increase in oscillator strength with n observed in linear molecules based on C_N (Maier 1998; Pino et al. 2001; Rice & Maier 2013).

For $2n \geq 8$, instead, two determinants contribute to the low-energy relevant peaks (Table E.1). The wavefunction, the transition dipole moment and its squared value, and the total energy assume the forms

$$|\psi\rangle \approx A_1|\psi^{(1)}\rangle + A_2|\psi^{(2)}\rangle\,, \tag{E.4}$$

$$d \approx A_1\psi_{GS}\,\mathbf{r}\psi^{(1)} + A_2\psi_{GS}\,\mathbf{r}\psi^{(2)} = d_1 + d_2\,, \tag{E.5}$$

$$\begin{aligned} d^2 &\approx A_1^2 \left|\psi_{GS}\,\mathbf{r}\psi^{(1)}\right|^2 + A_2^2 \left|\psi_{GS}\,\mathbf{r}\psi^{(2)}\right|^2 \\ &+ 2A_1A_2\psi^{(1)}\mathbf{r}\psi_{GS}\,\psi_{GS}\,\mathbf{r}\psi^{(2)}\,, \end{aligned} \tag{E.6}$$

$$\begin{aligned} E &= \psi\mathbf{H}\psi \\ &\approx A_1^2E_1 + A_2^2E_2 + 2A_1A_2\psi^{(1)}\mathbf{H}\psi^{(2)} \end{aligned} \tag{E.7}$$

if the coefficients and the determinants are real.

In particular, for the C_n-2P series with $2n \geq 8$, the TDDFT calculations predict that the first and second relevant excitations (at fixed n) are contributed to by the same transitions (i.e. same determinants), but with different amplitudes and with the opposite sign of the A_1A_2 product for the two excitations (Table E.1). Knowing the transition dipole moment d of each excitation, it is possible to invert the system of the two E.5 equations and obtain d_1 and d_2. For $2n = 8$, the product d_1d_2 is negative which, combined with the positive A_1A_2 term in the first excitation, results in a smaller oscillator strength for the first excitation with respect to the second one, according to Eq. E.6. For $2n \geq 10$, d_1d_2 is positive but the negative sign of A_1A_2 for the first excitation still results in a smaller oscillator strength.

Most important, these considerations on the sign of coefficients and transition dipole moments can explain the counterintuitive decrease in the oscillator strength of the first excitation as n increases. Since the product $A_1A_2d_1d_2$ in Eq. E.6 is always negative (for $2n \geq 8$), then the corresponding oscillator strength decays with n because $|A_1| \to |A_2|$. On the other hand, and for the same reason, the oscillator strength of the second excitation increases with n, as observed in the computed TDDFT spectra.

Table E.1. Details of the low-energy relevant TDDFT excitations of the C_{2n}-2P molecules ([a]).

	1st relevant peak						2nd relevant peak					
$2n$	E (eV)	f	d	Main contributions	A_i	A_i^2	E (eV)	f	d	Main contributions	A_i	A_i^2
4	3.87	0.81	2.924	HOMO–2 → LUMO	0.828	69%	5.46	3.09	4.804	HOMO–4 → LUMO+16	0.574	33%
6	3.48	0.87	3.195	HOMO–2 → LUMO	0.788	87%	4.89	5.53	-6.793	HOMO–4 → LUMO+4	0.656	43%
8	3.14	0.52	-2.609	HOMO → LUMO	-0.730	53%	4.53	7.39	8.160	HOMO → LUMO	0.520	27%
				HOMO–3 → LUMO+3	-0.531	28%				HOMO–3 → LUMO+3	-0.643	41%
10	2.87	0.32	2.126	HOMO → LUMO	0.695	48%	4.27	9.07	-9.316	HOMO → LUMO	-0.546	30%
				HOMO–3 → LUMO+1	-0.575	33%				HOMO–3 → LUMO+1	-0.626	39%
12	2.66	0.20	-1.764	HOMO → LUMO	-0.671	45%	4.05	6.85	-8.311	HOMO → LUMO	-0.542	29%
				HOMO–3 → LUMO+1	0.598	36%				HOMO–3 → LUMO+1	-0.577	33%
14	2.50	0.14	-1.490	HOMO → LUMO	-0.653	43%	3.88	9.09	9.778	HOMO → LUMO	0.557	31%
				HOMO–3 → LUMO+1	0.609	37%				HOMO–3 → LUMO+1	0.588	35%
20	2.21	0.05	0.987	HOMO → LUMO	0.612	37%	3.46	7.53	-9.431	HOMO → LUMO	-0.447	20%
				HOMO–3 → LUMO+1	-0.610	37%				HOMO–3 → LUMO+1	-0.468	22%
										HOMO–4 → LUMO+2	0.462	21%
	1st relevant peak						3rd relevant peak					
30	2.02	0.02	0.562	HOMO → LUMO	-0.550	30%	3.31	18.79	15.220	HOMO → LUMO	-0.554	31%
				HOMO–3 → LUMO+1	0.580	34%				HOMO–3 → LUMO+1	-0.583	34%

Notes. For each absorption peak, the peak energy (E, eV), the oscillator strength (f), transition dipole moment (d), the main contributions to the excitation with their amplitudes (A_i), and their contribution to the excitation (A_i^2, in percent) are reported. For instance, the first excitation of the C_{10}-2P is contributed to at 48% by HOMO → LUMO and at 33% by HOMO–3 → LUMO+1, while the second excitation consists of 30% HOMO → LUMO and 39% of HOMO–3 → LUMO+1.